Stress Transfer Analyses In Cellulose Nanofiber/Montmorillonite Nanocomposites With X-Ray Diffraction And Investigation On Effects of Chemical Interaction Between Cellulose Nanofiber And Montmorillonite

Takuya Matsumoto
Kobe University
Sunichi Mori
Kobe University
Takuya Ohashi
Kobe University
Takashi Nishino (tnishino@kobe-u.ac.jp)
Kobe University https://orcid.org/0000-0002-5095-9944

Research Article

Keywords: cellulose nanofiber, montmorillonite, nanocomposite, stress transfer, X-ray diffraction

Posted Date: June 21st, 2021

DOI: https://doi.org/10.21203/rs.3.rs-579612/v1

Abstract

Cellulose nanofiber is one of the promising materials for its eco-friendliness as well as high mechanical performance and high functionalities. Nanocomposites with cellulose nanofiber matrixes and inorganic nanofillers also possess more excellent mechanical properties by the reinforcement effects of the nanofillers. The mechanical reinforcement effects depend in a large part on the interfacial interaction between the nanofillers and the cellulose matrixes and the dispersion of the nanofiller in the nanocomposites. The quantitative evaluation of the reinforcement effects is insufficient, which is desired for the material design of industrial use of the cellulose composites. In this study, we used nanocomposites of cellulose nanofibers and montmorillonite with various surface properties. Their mechanical properties were investigated through tensile tests and the stress transfer to the nanofillers in nanocomposites with various combinations of cellulose nanofibers and nanofillers was analyzed through the X-ray diffraction method. The strong correlation between Young's modulus and stress transfer coefficients was revealed. In particular, the composites of TEMPO-oxide cellulose nanofiber and ion-exchanged montmorillonite possessed not only the highest Young's modulus but also the largest stress transfer coefficients. The large mechanical reinforcement effect of the loaded montmorillonite filler was observed and was attributed to the electrostatic interaction of the interface between the cellulose matrix and the montmorillonite filler.

Introduction

Cellulose nanocomposites have received much attention as environmental-friendly "green" materials. (Eichhorn et al. 2010; Cherian et al. 2011; Abdul Khalil et al. 2012; Oksman et al. 2016; Khattab et al. 2017; Chakrabarty and Teramoto 2018) The cellulose nanocomposites are categorized into two types. One is nanocomposites including cellulose as nanofillers, and the other includes as matrixes. In the nanocomposites including nanocellulose as fillers, conventional polymer resins as matrixes have been combined with cellulose nanocrystal (CNC)(Favier et al. 1995; Paralikar et al. 2008; Pei et al. 2011; Xu et al. 2013; Lin and Dufresne 2013; Arrieta et al. 2014; Kargarzadeh et al. 2015, 2017) and nanofiber (CNF) (Shimazaki et al. 2007; Jonoobi et al. 2010; Peresin et al. 2010; Sehaqui et al. 2012; Isogai 2013; Kargarzadeh et al. 2017) as mechanical reinforcement fillers. In these cases, *isotactic* polypropylene, (Wang and Sain 2007; Han et al. 2012; Yang et al. 2013; Iwamoto et al. 2014; Wang et al. 2018) polyethylene,(Wang and Sain 2007; Kiziltas et al. 2016; Sakakibara et al. 2017) poly(lactic acid),(Iwatake et al. 2008; Jonoobi et al. 2010; Wang and Drzal 2012; Kose and Kondo 2013) polyamide(Lee et al. 2011, 2014; Hivechi et al. 2019, 2020) have been reported as matrix polymers. Cellulose-matrix composites have also gathered much attention.(Sehaqui et al. 2010, 2012; Liu et al. 2011; Schütz et al. 2012; Liimatainen et al. 2013; Castro et al. 2018; González del Campo et al. 2018; Morimune-Moriya et al. 2018; Silva et al. 2019; Ito et al. 2019; Kato et al. 2019) In resin-impregnated wood texture,(Cabane et al. 2016; Li et al. 2016, 2018; Frey et al. 2018; Chen et al. 2019) hemicellulose and lignin were removed from wood textures without the destruction of their wood structure and precursors of polymer resins were penetrated into porous structure of the textures. The incorporation with wood textures and polymers was accessible

to high mechanical performance of the composite materials. Moreover, it has been investigated that the nanofillers in various cellulose composites provided the further mechanical reinforcements to nanocellulose-based materials with high modulus. The reinforcement effects directly depended on the modulus and the shape of the loaded fillers. Isogai, Saito and co-workers have been reported on oxidized CNF/montmorillonite (MMT) composites and investigated on their high Young's modulus and tensile strength and their excellent gas barrier properties.(Wu et al. 2012) MMT with two dimensional structure is originated from cray mineral, and is accepted as one of typical reinforcement fillers in nanocomposites. (Usuki et al. 1993; Liu et al. 2011; Wu et al. 2012) Because single nanofiber of cellulose itself inherently possesses high modulus even without any reinforcement fillers,(Sakurada et al. 1962; Nishino et al. 1995; Cheng and Wang 2008; Zhai et al. 2018) the mechanical properties of CNF/MMT composites were reinforced more largely by loading MMT fillers. Therefore, CNF/MMT composites have large advantages from the perspective of excellent mechanical performance as well as environmental friendly "all-green" composite materials.

It is well-known that the reinforcement effect in nanocomposites was provided from not only their high Young's modulus and the dispersibility of the loaded nanofillers but also the interfacial interaction between matrix polymers and inorganic fillers.(Komarneni 1992; Hussain et al. 2006; Camargo et al. 2009; Miculescu et al. 2016) The reinforcement effect and the stress concentration are evaluated as stress transfer from matrixes to nannofillers. The effective stress transfer is attributed to the strong interfacial interaction between fillers and matrixes, which leads to larger reinforcement effects. Therefore, the stronger interaction at interface between fillers and matrixes is significant. For the investigation on stress transfer in composites, X-ray diffraction measurements(Nakamae et al. 1992; Xu et al. 1992; Nishino et al. 1998, 2000, 2001, 2006; Morimune et al. 2010; Nishino 2012) and Raman scattering spectroscopic measurements(Young and Eichhorn 2007; Lachman et al. 2009; Young et al. 2012; Li et al. 2013) have been developed. In these measurements, the stress transfer is evaluated quantitatively from the shift of diffraction peaks and Raman scattering bands. These methods access to the molecular-scale analyses of stress transfer and lead to the direct evaluation of interfacial interaction. Actually, our group previously reported on large stress transfer from poly(vinyl alcohol) (PVA) matrix to MMT filler with X-ray diffraction analyses(Morimune et al. 2010). The large reinforcement effect was attributed to the strong interaction between the hydrophilic hydroxyl side chains of PVA and hydrophilic surface of MMT.

Herein, we focus on stress transfer of CNF/MMT composites with X-ray diffraction analyses. CNFs and MMTs with various surface properties are available. In the case of CNFs, neutral CNF is obtained through mechanical fibrillation with micro-fluidics,(Wang et al. 2015; Taheri and Samyn 2016) whereas, when CNF is oxidized with 2,2,6,6-tetramethylpiperidine 1-oxyl (TEMPO) at 6-position of glucopyranose rings, TEMPO-oxidized CNF (TOCN) with carboxylate anion is obtained.(Isogai et al. 2011) MMT possesses sodium cation in the interlayer. The cation is exchanged rapidly with other organic cation such as tetra alkyl ammonium through intercalation. We prepare nanocomposites with various combinations using their MMTs and CNFs. Their structure and mechanical properties of the obtained composites is investigated in the bulk scale. The mechanical reinforcement effect of MMTs in composites is evaluated from the perspective of stress transfer involving various interfacial interaction.

Materials And Methods

Materials

MMT powder “Kunipia-G” was supplied from Kunimine Industries Co., Ltd.. Tetraethylammonium hydroxide solution (Nacalai Tesque, Inc.) was used for exchanging interlayer cation of MMT. The refined pulp was prepared from Kenaf bast fibers (Toyota Boshoku Co., Ltd.), which were accepted as fillers of composites of structural materials in motor vehicle industry, through degreasing, Wise method, and alkaline treatment, according to the literatures(Nobuta et al. 2016). All the chemical products were purchased from chemical suppliers, and were used without any further purification.

Ion exchange of MMT

In exchange of MMT was performed based on the method reported by Jinnai and co-workers(Janeba et al. 1998). MMT powder 0.6 g was added to 120 mL of distilled water and the aqueous dispersion was stirred for 1 day to obtain 0.5 wt% of MMT dispersion. Aside from this, 0.8 g of 10 wt% tetraethylammonium hydroxide solution was added to the prepared MMT dispersion and the mixture dispersion was stirred for 2 h for the cation-exchange of the MMT interlayer. MMT-N^+Et_4 aqueous dispersion was obtained.

Preparation of FCN film and FCN/MMT composites

At first, 0.5 wt% refined kenaf in aqueous dispersion was pulverized by a high-speed mixer (Xtreme Hi-Power Blender, MX1200XT, Waring, U.S.A.) at 22,000 rpm for 10 min. After this pulverization step, the aqueous dispersion of refined kenaf fibers was passed through 10 times homogenization process with a high-pressure homogenizer (Microfluidizer® LM20, Microfluidics Inc., MA, U.S.A.) to obtain cellulose nanofibers (FCN).(Wang et al. 2015; Taheri and Samyn 2016) The process pressure was 207 MPa and the diameter of the chamber was 50 μm.

For the preparation of FCN/MMT composites, 6 g of 0.5 wt% dispersions of MMT was added into 300 g of 0.2 wt% of FCN aqueous dispersion. The weight ratio of MMT to FCN was adjusted to 5 wt%. The nanocomposites were obtained by filtration on a PTFE membrane filter, drying under vacuum pressure at 40 ºC for over 12 h, and hot-pressing at 1 MPa, 120 ºC for 1 h. FCN/MMT-N^+Et_4 composites was also obtained through the similar process to the FCN/MMT composite.

Preparation of TOCN film and TOCN/MMT composites

TOCN was prepared in the methods reported by Isogai, Saito and co-workers(Isogai et al. 2011). Both the nanocomposites of the TOCN/MMT, and TOCN/MMT-N^+Et_4 were also obtained with the similar process to the FCN/MMT composite.

Measurement of thermal decomposition behavior

Thermal gravimetric analyses (TGA) of FCN and TOCN sheets and their composites were performed with Thermo plus EVO2 TG8121 (Rigaku) under nitrogen gas. The flow rate of nitrogen gas was 200 mL/min, the heating rate was 10°C/min, and the scanning of temperature was from room temperature to 500°C. To exclude water contained in the measurement samples, the samples was dried over under vacuum at 40°C for longer than 6 h and was remained at 120°C for 30 min before measurements. The temperature where the 5 wt% of the sample weight was lost compared to those at 150°C was defined as the thermal decomposition temperature (T_{d5}).

Measurements of X-ray diffraction

X-ray diffraction profiles of MMT powders, CNF sheets and the composites were measured with RINT2100 (Rigaku) in the $\theta/2\theta$ method. The X-ray beam was generated with 40 kV and 20 mA and the wavelength was 1.5418 Å (CuKα). The scanning rate was 2°/min, the step was 0.02°, and the scanning range of 2θ was from 3° to 40°.

Measurements of two-dimentional X-ray diffraction

Two-dimentional X-ray diffraction profiles of the CNF sheets and the composites were measured with RINT2000 (Rigaku) in the transmittance method. The X-ray beam was generated with 40 kV and 20 mA and the wavelength was 1.5418 Å (CuKα). The camera distance was 56.3 mm. The irradiation time of X-ray beam was 20 min. The X-ray beam was irradiated into the sample films from the direction perpendicular or parallel to the surface of the samples and the diffraction was detected with imaging plates. From the measurements with these geometries, the in-plane or through-plane orientation of the crystallites were evaluated.

Measurements of mechanical properties

Tensile tests were performed with autograph AG-X plus (Shimadzu). The samples were trimmed into 30 mm · 5 mm rectangles, the initial length in the tensile test was 10 mm and the tensile speed was 0.5 mm/min. The densities of the films were evaluated in the floating method using calcium chloride aqueous solution at 30°C. The cross sectional area was calculated from the densities and the weight and the length of samples. In order to obtain reliable data, we performed tensile tests of more than five specimens for every sample, and averaged their obtained mechanical properties.

Stress transfer analyses of composites with X-ray diffraction

X-ray diffraction measurements for stress transfer analyses was performed with RINT2000 (Rigaku) in the symmetric transmittance method using CuKα beam (1.5418 Å). The X-ray beam was generated with 40 kV and 20 mA and the wavelength 1.5418 Å (CuKα). The scanning rate is 0.1°/min, the step was 0.006°, and the scanning range of 2θ was from 61° to 63°. The samples were trimmed into 30 mm · 5 mm rectangles. The samples were set in a stretching device and the stress was measured with a load cell LUB-B (Kyowa Electronic Instruments). The tensile apparatus put on the gonio stage of the X-ray

diffractometer. Under applying tensile stress to the samples, the X-ray diffraction peaks were evaluated. In the case of the CNF/MMT composites, we focused on the shift of diffraction peaks originated from (060) plane of MMT. The strain of MMT crystallite ε_c was calculated from the lattice distance d_0 of (060) plane before loading and the difference of the lattice distance Δd from the diffraction peaks before and under loading, according to the below Eq. (1). In addition, from the Eq. (2), the stress σ_c transferred to the MMT nanofiller and the stress concentration coefficient σ_c/σ_0 were estimated.

$$\varepsilon_c = \Delta d / d_0 \quad (1)$$

$$\sigma_c = \varepsilon_c \cdot E_{(060)} \quad (2)$$

where $E_{(060)}$ is the elastic modulus of MMT crystal for the (060) plane of MMT, and σ_0 is the stress applied to the whole sample. The $E_{(060)}$ of MMT was 400 GPa.(Manevitch and Rutledge 2004)

Results And Discussion

The FCN and TOCN as matrixes in the composites were prepared from the kenaf pulps through mechanical and chemical nanofibrillization with microfluidics method and TEMPO oxidation, respectively. The characterization of the obtained CNF are shown in Figure S1 in the Supporting Information. For the investigation of diameters of the CNF, AFM observation was performed. From the height of the CNF in the topological images, it was revealed that the diameters of nanofibers of FCN and TOCN were 19 ± 6.8 nm and 2.7 ± 0.5 nm. FCN was a bundle of single cellulose fibers, while TOCN stood as a single elementary fibril. In the FTIR spectra of FCN and TOCN in Figure S1e in the Supporting Information, the absorption band of carboxyl groups at 6-position of TEMPO-oxidized cellulose were appeared at 1610 cm^{-1}, whereas no band of carboxyl groups in the non-fibrillated refined pulp and FCN was observed. For the quantitative estimation of the oxidation of hydroxyl groups of their CNF, conductometric titration was performed, as shown in in Figure S1f in the Supporting Information. As this result, TOCN possessed carboxyl groups in the concentration of 1.66 mol/g-cellulose. In contrast, the concentration of carboxyl groups in FCN was only 0.14 mol/g-cellulose. This means that the oxidation of hydroxyl groups at 6-position of cellulose was progressed and 81% of hydroxyl groups at 6-position at the surface of the Isogai and Saito's cellulose crystallite model(Daicho et al. 2018, 2020) was converted to carboxyl groups. In X-ray diffraction profiles of both the CNF, the diffraction peaks of type I_β of cellulose crystal were observed at 14.9° and 22.5°. This suggested that, even after mechanical and chemical nanofibrillization, crystalline structure of cellulose in CNF kept unchanged.

Ion exchange of sodium cations to tetraethyl ammonium ions in MMT was performed with the addition of tetraethyl ammonium hydroxide into MMT aqueous dispersion. Figure 1a shows X-ray diffraction profiles of MMT and ion-exchanged MMT (MMT-NEt_4^+). In the profiles, the 001 reflection of MMT at 7.2° were completely shifted to 6.3° after the ion exchange (Stathi et al. 2007), which indicates the interlayer

distance was increased by intercalation of tetraethyl ammonium ion larger than sodium ion. The ion exchange converted all the MMT to MMT-NEt_4^+.

Table 1
Decomposition temperature and fraction ratios of MMT of FCN, FCN/MMT, FCN/MMT-N^+Et_4, TOCN, TOCN/MMT and TOCN/MMT-N^+Et_4 composites.

Sample	T_{d5}	MMT content vs. cellulose
	°C	wt%
FCN	273	-
FCN/MMT	278	2.83
FCN/MMT-N^+Et_4	275	2.81
TOCN	232	-
TOCN/MMT	233	3.81
TOCN/MMT-N^+Et_4	235	3.70

In the preparation of CNF/MMT composites, the mixture method of CNF and MMT in aqueous dispersion was employed because both the matrixes of CNF and fillers of MMT were well dispersed into water. After slow filtration, the composite films were obtained. For the investigation of thermal stabilities of the composites and the amounts of MMT fillers in the composites, their thermal gravimetric behaviors were measured. The decomposition temperature T_{d5} was increased by loading the MMT fillers in the both composites. The FCN/MMT was decomposed at higher temperature than FCN/MMT-NEt_4^+, while T_{d5} of TOCN/MMT-NEt_4^+ was higher than that of TOCN/MMT. It is suspected that the interaction of MMT fillers with CNF matrixes would decide their decomposition behavior because the molecular motions of CNF matrixes was restricted by the MMT filler.

From the residual weight at 500°C, the weight fractions of MMT fillers in the composites were estimated as around 3 wt%. This value approximately coincided to the mixture ratio in preparation recipe, which suggests MMT in CNF/MMT mixed dispersion passed through the filter under filteration. In addition, from the X-ray diffraction profiles of the prepared composites as shown in Fig. 1b, both the diffraction peaks originated from CNF and MMT were observed in all the composites. The structure of cellulose I_β crystallites and layered structure of MMT fillers were both remained even after preparation of their composites. Moreover, the 100 reflection of MMT in both FCN and TOCN composites were broadened and weakened relative to those of MMT-NEt_4^+. This result reveals that MMT in composites was exfoliated or

intercalated by CNF and the distance between MMT layers was increased. In contrast, the ion-exchanged MMT-NEt_4^+ even in composites remained rigid layered structure of MMT-NEt_4^+ itself.

For the evaluation of the structural orientation of the composites, two-dimensional X-ray diffraction were measured with two geometries. Figure 2 showed 2D X-ray diffraction images of the CNF/MMT composites when the X-ray beam was irradiated from the “through” direction perpendicular to the surface, and “edge” direction parallel to the surface. In the “through” images of all the composites, Debye-Sherrer rings of 110/1–10 and 200 reflections of cellulose were observed, while, in the edge diffraction images, not only the diffractions of cellulose but also 001 reflection of MMT fillers were detected as arcs on the meridional direction. This suggested that, in all the composites, the cellulose nanofibers as well as fillers were oriented. The fiber axis and the MMT plane were oriented to the direction parallel to the surface because these composites were prepared by slow filtration from CNF/MMT aqueous dispersion. Compared with FCN composites, it is revealed that the in-plane orientation of TOCN in TOCN/MMT and TOCN/MMT-N^+Et_4 composites were increased judging from sharper arc of reflection of cellulose in their edge diffraction images.

Figure 3 shows the schematic structure model of CNF matrixes and MMT fillers in the composites observed from in-plane and edge directions. The in-plane structures of all the prepared composites were random and isotropic. In the view of edge side of the composites with FCN matrix, the fibers of FCN were mainly oriented but some possessed disordered structure, whereas the TOCN-based composites possessed the highly oriented structure. This enhanced in-plane orientation of TOCN should be attributed to the smaller diameters and higher aspect ratios of TOCN. In addition, from the results of X-ray diffraction profiles of the composites, the 2D plates of MMT in both the CNFs composites were more exfoliated and isolated rather than those of MMT-N^+Et_4 and the MMT planes in the all the composites were laid parallel to the surface of the composite films.

For the investigation on the mechanical properties, tensile tests of the CNF sheets and composites were performed. The strain-stress curves and parameters of the mechanical properties of the CNF/MMT composites were shown in Fig. 4 and Table 2, respectively. All the TOCN films and composites possessed higher Young’s modulus than FCN ones, which were attributed to the lower diameters and higher aspect ratios of TOCN.(Henriksson et al. 2008) In the case of FCN matrixes, the composites with MMT possessed larger Young’s modulus than that with MMT-N^+Et_4. This reason would be that MMT in the FCN/MMT composite was a single-layer-like structure as suggested from its X-ray diffraction profile and possessed large contact area with FCM matrix, compared with MMT-N^+Et_4. In contrast, the Young’s modulus of the TOCN/MMT-N^+Et_4 composite was larger than those of the TOCN/MMT composites because carboxylate anions of TOCN, not FCN, would possess strong interaction with ammonium cations of MMT-N^+Et_4. This would be attributed to the larger hydrophobic affinity of N^+Et_4 with the glucopyranose rings of cellulose. It is concluded that the TOCN/MMT-N^+Et_4 composite have the largest mechanical reinforcement effects.

Table 2
Mechanical properties of FCN, FCN/MMT, FCN/MMT-N^+Et_4, TOCN, TOCN/MMT, and TOCN/MMT-N^+Et_4 films.

Sample	Young's modulus	Tensile strength	Elongation at break
	GPa	MPa	%
FCN	9.5 ± 0.2	249 ± 9	5.8 ± 0.3
FCN/MMT	13.5 ± 0.9	301 ± 41	3.9 ± 1.0
FCN/MMT-N^+Et_4	11.1 ± 2.5	224 ± 76	3.1 ± 1.1
TOCN	12.2 ± 0.8	238 ± 24	4.9 ± 0.8
TOCN/MMT	14.8 ± 0.6	213 ± 47	1.7 ± 0.5
TOCN/MMT-N^+Et_4	16.5 ± 0.4	287 ± 27	2.4 ± 0.4

To reveal the mechanical reinforcement effects of MMT fillers in CNF composites, stress transfer to the MMT fillers in their composites were evaluated in the X-ray diffraction method under loading tensile stress. When the mechanical stress was loaded to the CNF/MMT composite, the diffraction peak of (060) plane was shifted to the lower angles, as shown in Figure S3 in the Supporting Information. This means the increase of the lattice spacing with loading tensile stress. Because the MMT fillers were dispersed in the CNF composites in the parallel to the composite surface and the (060) plane received tensile stress in perpendicular direction, the lattice strains were directly calculated from the shifts of the diffraction peek and the elastic modulus of the (060) plane of MMTs. In addition, the comparison between the estimated stress of MMT fillers and the mechanically applied stress of the composites provided the stress transfer effects from the composite bulks to the MMT fillers and mechanical reinforcement effects of the MMT fillers with the dependence of interfacial interaction.

The stress on the MMT fillers in the four composites were evaluated under applying different tensile stress. Figure 5 shows the plots of the stress on the MMT fillers for the various applied stress to the whole composite films. The inclination of the obtained approximate straight lines to the plots provided stress transfer coefficients σ_c/σ_0 from composites to fillers. The stress-transfer coefficients σ_c/σ_0 of all the CNF/MMT composites are also shown in Fig. 5. The coefficients σ_c/σ_0 of FCN/MMT-N^+Et_4, FCN/MMT, TOCN/MMT and TOCN/MMT-N^+Et_4, in that order, increased, which was the same as the order of their Young's modulus. The TOCN/MMT-N^+Et_4 composite possessed the largest value of the stress-transfer coefficient and the MMT-N^+Et_4 fillers received 16 times lager stress than the whole TOCN/MMT-N^+Et_4 composites. This means that the applied stress was concentrated most highly to the MMT-N^+Et_4 fillers and the largest stress concentration would lead to the largest Young's modulus, as shown in Fig. 6. The reason for this largest stress-transfer coefficient of the TOCN/MMT-N^+Et_4 composite is suspected that the carboxylate anions of the TOCN matrix would be possessed the stronger electrostatic interaction with the

ammonium cations of the MMT-N^+Et_4 fillers, relative to the other CNF/MMT composites. In the case of the TOCN/MMT composite, as the MMT included sodium cation, the interfacial interaction between TOCN and MMT was decreased and this stress-transfer coefficient was lower relative to the TOCN/MMT-N^+Et_4 composite. Moreover, because FCN without any ionic moiety possessed weaker interaction with MMT fillers, the stress-transfer coefficients of the FCN composites were lower than the TOCN composites. In particular, MMT-N^+Et_4 fillers were exfoliated deficiently in the FCN/MMT-N^+Et_4 composite. Therefore, the MMT-N^+Et_4 fillers would behave as defects in the composite partially, and then the value of the stress-transfer coefficients of the FCN/MMT-N^+Et_4 composite was lowest.(Kawasumi et al. 1997; Hasegawa et al. 1998)

Conclusions

We demonstrated stress transfer analyses in CNF/MMT composites with X-ray diffraction. The MMT fillers reinforced the mechanical properties of CNF materials sufficiently. The mechanical reinforcement effects were controlled by the combination of various CNF matrixes and MMT fillers. We evaluated the reinforcement effects of CNF/MMT composites with the various combinations. The Young's modulus of the TOCN/MMT-N^+Et_4 composite was the largest. Form the quantitative stress transfer analyses using X-ray diffraction, the stress-transfer coefficient of the TOCN/MMT-N^+Et_4 composite was also larger than any other composites. The strong correlation between Young's modulus and stress-transfer coefficients was revealed, including the cases of CNF/MMT composites with the other combination. In addition, it is suspected that the stress-transfer coefficients of the CNF/MMT composites depended on the interfacial interaction between the CNF matrixes and MMT fillers.

Declarations

ASSOCIATED CONTENT

Supplementary data.

The experimental procedure of FT-IR measurements and AMF observation, AFM topological images, FT-IR spectra, conductometric titrimetric profiles, thermo-gravimetric traces, and X-ray diffraction profiles under stress transfer analyses are described in the Supplementary data.

AUTHOR INFORMATION

Corresponding Author

*(T.N.) E-mail: tnishino@kobe-u.ac.jp

Funding Sources

This work was supported by the Core Research for Evolutional Science and Technology (CREST, JPMJCR13B2), and Japan Science and Technology Agency.

Notes

The authors declare no competing financial interest.

Compliance with Ethical Standards

The authors declare no conflicts of interest. This paper not included a research involving human participants and/or animals. The authors promised informed consent.

References

1. Abdul Khalil HPS, Bhat AH, Ireana Yusra AF (2012) Green composites from sustainable cellulose nanofibrils: A review. Carbohydr Polym 87:963–979. https://doi.org/https://doi.org/10.1016/j.carbpol.2011.08.078
2. Arrieta MP, Fortunati E, Dominici F et al (2014) Multifunctional PLA–PHB/cellulose nanocrystal films: Processing, structural and thermal properties. Carbohydr Polym 107:16–24. https://doi.org/https://doi.org/10.1016/j.carbpol.2014.02.044
3. Cabane E, Keplinger T, Künniger T et al (2016) Functional lignocellulosic materials prepared by ATRP from a wood scaffold. Sci Rep 6:31287. https://doi.org/10.1038/srep31287
4. Camargo PHC, Satyanarayana KG, Wypych F (2009) Nanocomposites: synthesis, structure, properties and new application opportunities. Mater Res 12:1–39
5. Castro DO, Karim Z, Medina L et al (2018) The use of a pilot-scale continuous paper process for fire retardant cellulose-kaolinite nanocomposites. Compos Sci Technol 162:215–224. https://doi.org/https://doi.org/10.1016/j.compscitech.2018.04.032
6. Chakrabarty A, Teramoto Y (2018) Recent Advances in Nanocellulose Composites with Polymers: A Guide for Choosing Partners and How to Incorporate Them. Polymers (Basel) 10:517. https://doi.org/10.3390/polym10050517
7. Chen H, Baitenov A, Li Y et al (2019) Thickness Dependence of Optical Transmittance of Transparent Wood: Chemical Modification Effects. ACS Appl Mater Interfaces 11:35451–35457. https://doi.org/10.1021/acsami.9b11816
8. Cheng Q, Wang S (2008) A method for testing the elastic modulus of single cellulose fibrils via atomic force microscopy. Compos Part A Appl Sci Manuf 39:1838–1843. https://doi.org/https://doi.org/10.1016/j.compositesa.2008.09.007
9. Cherian BM, Leao AL, de Souza SF et al (2011) Cellulose Nanocomposites for High-Performance Applications BT - Cellulose Fibers: Bio- and Nano-Polymer Composites: Green Chemistry and Technology. In: Kalia S, Kaith BS, Kaur I (eds). Springer Berlin Heidelberg, Berlin, pp 539–587

10. Daicho K, Kobayashi K, Fujisawa S, Saito T (2020) Crystallinity-Independent yet Modification-Dependent True Density of Nanocellulose. Biomacromol 21:939–945. https://doi.org/10.1021/acs.biomac.9b01584
11. Daicho K, Saito T, Fujisawa S, Isogai A (2018) The Crystallinity of Nanocellulose: Dispersion-Induced Disordering of the Grain Boundary in Biologically Structured Cellulose. ACS Appl Nano Mater 1:5774–5785. https://doi.org/10.1021/acsanm.8b01438
12. Eichhorn SJ, Dufresne A, Aranguren M et al (2010) Review: current international research into cellulose nanofibres and nanocomposites. J Mater Sci 45:1–33. https://doi.org/10.1007/s10853-009-3874-0
13. Favier V, Chanzy H, Cavaille JY (1995) Polymer Nanocomposites Reinforced by Cellulose Whiskers. Macromolecules 28:6365–6367. https://doi.org/10.1021/ma00122a053
14. Frey M, Widner D, Segmehl JS et al (2018) Delignified and Densified Cellulose Bulk Materials with Excellent Tensile Properties for Sustainable Engineering. ACS Appl Mater Interfaces 10:5030–5037. https://doi.org/10.1021/acsami.7b18646
15. González del Campo MM, Darder M, Aranda P et al (2018) Functional Hybrid Nanopaper by Assembling Nanofibers of Cellulose and Sepiolite. Adv Funct Mater 28:1703048. https://doi.org/10.1002/adfm.201703048
16. Han T-H, Lee Y, Choi M-R et al (2012) Extremely efficient flexible organic light-emitting diodes with modified graphene anode. Nat Photonics 6:105
17. Hasegawa N, Kawasumi M, Kato M, et al (1998) Preparation and mechanical properties of polypropylene-clay hybrids using a maleic anhydride-modified polypropylene oligomer. J Appl Polym Sci 67:87–92. https://doi.org/10.1002/(SICI)1097-4628(19980103)67:1<87::AID-APP10>3.0.CO;2-2
18. Henriksson M, Berglund LA, Isaksson P et al (2008) Cellulose Nanopaper Structures of High Toughness. Biomacromol 9:1579–1585. https://doi.org/10.1021/bm800038n
19. Hivechi A, Bahrami SH, Siegel RA (2019) Drug release and biodegradability of electrospun cellulose nanocrystal reinforced polycaprolactone. Mater Sci Eng C 94:929–937. https://doi.org/https://doi.org/10.1016/j.msec.2018.10.037
20. Hivechi A, Bahrami SH, Siegel RA et al (2020) In vitro and in vivo studies of biaxially electrospun poly(caprolactone)/gelatin nanofibers, reinforced with cellulose nanocrystals, for wound healing applications. Cellulose 27:5179–5196. https://doi.org/10.1007/s10570-020-03106-9
21. Hussain F, Hojjati M, Okamoto M, Gorga RE (2006) Review article: Polymer-matrix Nanocomposites, Processing, Manufacturing, and Application: An Overview. J Compos Mater 40:1511–1575. https://doi.org/10.1177/0021998306067321
22. Isogai A (2013) Wood nanocelluloses: fundamentals and applications as new bio-based nanomaterials. J Wood Sci 59:449–459. https://doi.org/10.1007/s10086-013-1365-z
23. Isogai A, Saito T, Fukuzumi H (2011) TEMPO-oxidized cellulose nanofibers. Nanoscale 3:71–85
24. Ito H, Sakata M, Hongo C et al (2019) Cellulose nanofiber nanocomposites with aligned silver nanoparticles. Nanocomposites 1–11. https://doi.org/10.1080/20550324.2018.1556912

25. Iwamoto S, Yamamoto S, Lee S-H, Endo T (2014) Solid-state shear pulverization as effective treatment for dispersing lignocellulose nanofibers in polypropylene composites. Cellulose 21:1573–1580. https://doi.org/10.1007/s10570-014-0195-5
26. Iwatake A, Nogi M, Yano H (2008) Cellulose nanofiber-reinforced polylactic acid. Compos Sci Technol 68:2103–2106. https://doi.org/https://doi.org/10.1016/j.compscitech.2008.03.006
27. Janeba D, Čapková P, Weiss Z (1998) Molecular Mechanics Studies of Montmorillonite Intercalated with Tetramethylammonium and Trimethylphenylammonium. Mol Model Annu 4:176–182. https://doi.org/10.1007/s0089480040176
28. Jonoobi M, Harun J, Mathew AP, Oksman K (2010) Mechanical properties of cellulose nanofiber (CNF) reinforced polylactic acid (PLA) prepared by twin screw extrusion. Compos Sci Technol 70:1742–1747. https://doi.org/https://doi.org/10.1016/j.compscitech.2010.07.005
29. Kargarzadeh H, Sheltami M, Ahmad R I, et al (2015) Cellulose nanocrystal: A promising toughening agent for unsaturated polyester nanocomposite. Polymer 56:346–357. https://doi.org/https://doi.org/10.1016/j.polymer.2014.11.054
30. Kargarzadeh H, Mariano M, Huang J et al (2017) Recent developments on nanocellulose reinforced polymer nanocomposites: A review. Polymer 132:368–393. https://doi.org/https://doi.org/10.1016/j.polymer.2017.09.043
31. Kato T, Matsumoto T, Hongo C, Nishino T (2019) Mechanical and thermal properties of cellulose nanofiber composites with nanodiamond as nanocarbon filler. Nanocomposites 1–10. https://doi.org/10.1080/20550324.2018.1550924
32. Kawasumi M, Hasegawa N, Kato M et al (1997) Preparation and Mechanical Properties of Polypropylene – Clay Hybrids. Macromolecules 30:6333–6338. https://doi.org/10.1021/ma961786h
33. Khattab MM, Abdel-Hady NA, Dahman Y (2017) 21 - Cellulose nanocomposites: Opportunities, challenges, and applications. In: Jawaid M, Boufi S, H.P.S. AKBT-C-RNC (eds) Woodhead Publishing Series in Composites Science and Engineering. Woodhead Publishing, pp 483–516
34. Kiziltas A, Nazari B, Kiziltas EE et al (2016) Cellulose NANOFIBER-polyethylene nanocomposites modified by polyvinyl alcohol. J Appl Polym Sci 133:. https://doi.org/10.1002/app.42933
35. Komarneni S (1992) Feature article. Nanocomposites. J Mater Chem 2:1219–1230. https://doi.org/10.1039/JM9920201219
36. Kose R, Kondo T (2013) Size effects of cellulose nanofibers for enhancing the crystallization of poly(lactic acid). J Appl Polym Sci 128:1200–1205. https://doi.org/10.1002/app.38308
37. Lachman N, Bartholome C, Miaudet P et al (2009) Raman Response of Carbon Nanotube/PVA Fibers under Strain. J Phys Chem C 113:4751–4754. https://doi.org/10.1021/jp900355k
38. Lee J-A, Yoon M-J, Lee E-S et al (2014) Preparation and characterization of cellulose nanofibers (CNFs) from microcrystalline cellulose (MCC) and CNF/polyamide 6 composites. Macromol Res 22:738–745. https://doi.org/10.1007/s13233-014-2121-y
39. Lee S-H, Teramoto Y, Endo T (2011) Cellulose nanofiber-reinforced polycaprolactone/polypropylene hybrid nanocomposite. Compos Part A Appl Sci Manuf 42:151–156.

https://doi.org/https://doi.org/10.1016/j.compositesa.2010.10.014

40. Li Y, Fu Q, Yu S et al (2016) Optically Transparent Wood from a Nanoporous Cellulosic Template: Combining Functional and Structural Performance. Biomacromol 17:1358–1364. https://doi.org/10.1021/acs.biomac.6b00145
41. Li Y, Yang X, Fu Q et al (2018) Towards centimeter thick transparent wood through interface manipulation. J Mater Chem A 6:1094–1101. https://doi.org/10.1039/C7TA09973H
42. Li Z, Young RJ, Kinloch IA (2013) Interfacial Stress Transfer in Graphene Oxide Nanocomposites. ACS Appl Mater Interfaces 5:456–463. https://doi.org/10.1021/am302581e
43. Liimatainen H, Ezekiel N, Sliz R et al (2013) High-Strength Nanocellulose–Talc Hybrid Barrier Films. ACS Appl Mater Interfaces 5:13412–13418. https://doi.org/10.1021/am4043273
44. Lin N, Dufresne A (2013) Physical and/or Chemical Compatibilization of Extruded Cellulose Nanocrystal Reinforced Polystyrene Nanocomposites. Macromolecules 46:5570–5583. https://doi.org/10.1021/ma4010154
45. Liu A, Walther A, Ikkala O et al (2011) Clay Nanopaper with Tough Cellulose Nanofiber Matrix for Fire Retardancy and Gas Barrier Functions. Biomacromol 12:633–641. https://doi.org/10.1021/bm101296z
46. Manevitch OL, Rutledge GC (2004) Elastic Properties of a Single Lamella of Montmorillonite by Molecular Dynamics Simulation. J Phys Chem B 108:1428–1435. https://doi.org/10.1021/jp0302818
47. Miculescu M, Thakur VK, Miculescu F, Voicu SI (2016) Graphene-based polymer nanocomposite membranes: a review. Polym Adv Technol 27:844–859. https://doi.org/10.1002/pat.3751
48. Morimune-Moriya S, Salajkova M, Zhou Q et al (2018) Reinforcement Effects from Nanodiamond in Cellulose Nanofibril Films. Biomacromol 19:2423–2431. https://doi.org/10.1021/acs.biomac.8b00010
49. Morimune S, Kotera M, Nishino T (2010) Stress Transfer of Poly (VinylAlcohol) / Montmorillonite Nano composite Using X-ray Diffraction. J Adhes Soc Japan 46:320–324. https://doi.org/10.11618/adhesion.46.320
50. Nakamae K, Nishino T, Airu X (1992) Studies on mechanical properties of polymer composites by X-ray diffraction: 3. Mechanism of stress transmission in particulate epoxy composite by X-ray diffraction. Polymer 33:2720–2724. https://doi.org/https://doi.org/10.1016/0032-3861(92)90444-2
51. Nishino T (2012) X-ray Diffraction Analyses on Stress Transfer Through Polymer Composites Interface. J Adhes Soc Japan 48:48–57. https://doi.org/10.11618/adhesion.48.48
52. Nishino T, Hirao K, Kotera M (2006) X-ray diffraction studies on stress transfer of kenaf reinforced poly(l-lactic acid) composite. Compos Part A Appl Sci Manuf 37:2269–2273. https://doi.org/https://doi.org/10.1016/j.compositesa.2006.01.026
53. Nishino T, Hirokane D, Nakamae K (2001) X-ray diffraction studies of the environmental deterioration of a transversely loaded carbon-fibre-reinforced composite. Compos Sci Technol 61:2455–2459. https://doi.org/https://doi.org/10.1016/S0266-3538(01)00174-9

54. Nishino T, Naito H, Nakamura K, Nakamae K (2000) X-ray diffraction studies on the stress transfer of transversely loaded carbon fibre reinforced composite. Compos Part A Appl Sci Manuf 31:1225–1230. https://doi.org/https://doi.org/10.1016/S1359-835X(00)00084-1
55. Nishino T, Takano K, Nakamae K (1995) Elastic modulus of the crystalline regions of cellulose polymorphs. J Polym Sci Part B Polym Phys 33:1647–1651. https://doi.org/10.1002/polb.1995.090331110
56. Nishino T, Tanaka T, Nakamae K (1998) Stress Transfer in High Performance Polyethylene Fiber Reinforced Epoxy Resin Composite Analyzed by X-Ray Diffraction. J Soc Mater Sci Japan 47:293–298. https://doi.org/10.2472/jsms.47.293
57. Nobuta K, Teramura H, Ito H et al (2016) Characterization of cellulose nanofiber sheets from different refining processes. Cellulose 23:403–414. https://doi.org/10.1007/s10570-015-0792-y
58. Oksman K, Aitomäki Y, Mathew AP et al (2016) Review of the recent developments in cellulose nanocomposite processing. Compos Part A Appl Sci Manuf 83:2–18. https://doi.org/https://doi.org/10.1016/j.compositesa.2015.10.041
59. Paralikar SA, Simonsen J, Lombardi J (2008) Poly(vinyl alcohol)/cellulose nanocrystal barrier membranes. J Memb Sci 320:248–258. https://doi.org/https://doi.org/10.1016/j.memsci.2008.04.009
60. Pei A, Malho J-M, Ruokolainen J et al (2011) Strong Nanocomposite Reinforcement Effects in Polyurethane Elastomer with Low Volume Fraction of Cellulose Nanocrystals. Macromolecules 44:4422–4427. https://doi.org/10.1021/ma200318k
61. Peresin MS, Habibi Y, Zoppe JO et al (2010) Nanofiber Composites of Polyvinyl Alcohol and Cellulose Nanocrystals: Manufacture and Characterization. Biomacromol 11:674–681. https://doi.org/10.1021/bm901254n
62. Sakakibara K, Moriki Y, Yano H, Tsujii Y (2017) Strategy for the Improvement of the Mechanical Properties of Cellulose Nanofiber-Reinforced High-Density Polyethylene Nanocomposites Using Diblock Copolymer Dispersants. ACS Appl Mater Interfaces 9:44079–44087. https://doi.org/10.1021/acsami.7b13963
63. Sakurada I, Nukushina Y, Ito T (1962) Experimental determination of the elastic modulus of crystalline regions in oriented polymers. J Polym Sci 57:651–660. https://doi.org/10.1002/pol.1962.1205716551
64. Schütz C, Sort J, Bacsik Z et al (2012) Hard and Transparent Films Formed by Nanocellulose–TiO2 Nanoparticle Hybrids. PLoS One 7:e45828
65. Sehaqui H, Ezekiel Mushi N, Morimune S et al (2012) Cellulose Nanofiber Orientation in Nanopaper and Nanocomposites by Cold Drawing. ACS Appl Mater Interfaces 4:1043–1049. https://doi.org/10.1021/am2016766
66. Sehaqui H, Liu A, Zhou Q, Berglund LA (2010) Fast Preparation Procedure for Large, Flat Cellulose and Cellulose/Inorganic Nanopaper Structures. Biomacromol 11:2195–2198. https://doi.org/10.1021/bm100490s

67. Shimazaki Y, Miyazaki Y, Takezawa Y et al (2007) Excellent Thermal Conductivity of Transparent Cellulose Nanofiber/Epoxy Resin Nanocomposites. Biomacromol 8:2976–2978. https://doi.org/10.1021/bm7004998
68. Silva JM, Barud HS, Meneguin AB et al (2019) Inorganic-organic bio-nanocomposite films based on Laponite and Cellulose Nanofibers (CNF). Appl Clay Sci 168:428–435. https://doi.org/https://doi.org/10.1016/j.clay.2018.12.003
69. Stathi P, Litina K, Gournis D et al (2007) Physicochemical study of novel organoclays as heavy metal ion adsorbents for environmental remediation. J Colloid Interface Sci 316:298–309. https://doi.org/https://doi.org/10.1016/j.jcis.2007.07.078
70. Taheri H, Samyn P (2016) Effect of homogenization (microfluidization) process parameters in mechanical production of micro- and nanofibrillated cellulose on its rheological and morphological properties. Cellulose 23:1221–1238. https://doi.org/10.1007/s10570-016-0866-5
71. Usuki A, Kojima Y, Kawasumi M et al (1993) Synthesis of nylon 6-clay hybrid. J Mater Res 8:1179–1184. DOI 10.1557/JMR.1993.1179
72. Wang B, Sain M (2007) Isolation of nanofibers from soybean source and their reinforcing capability on synthetic polymers. Compos Sci Technol 67:2521–2527. https://doi.org/https://doi.org/10.1016/j.compscitech.2006.12.015
73. Wang L, Okada K, Sodenaga M et al (2018) Effect of surface modification on the dispersion, rheological behavior, crystallization kinetics, and foaming ability of polypropylene/cellulose nanofiber nanocomposites. Compos Sci Technol 168:412–419. https://doi.org/https://doi.org/10.1016/j.compscitech.2018.10.023
74. Wang T, Drzal LT (2012) Cellulose-Nanofiber-Reinforced Poly(lactic acid) Composites Prepared by a Water-Based Approach. ACS Appl Mater Interfaces 4:5079–5085. https://doi.org/10.1021/am301438g
75. Wang W, Mozuch MD, Sabo RC et al (2015) Production of cellulose nanofibrils from bleached eucalyptus fibers by hyperthermostable endoglucanase treatment and subsequent microfluidization. Cellulose 22:351–361. https://doi.org/10.1007/s10570-014-0465-2
76. Wu C-N, Saito T, Fujisawa S et al (2012) Ultrastrong and High Gas-Barrier Nanocellulose/Clay-Layered Composites. Biomacromol 13:1927–1932. https://doi.org/10.1021/bm300465d
77. Xu A-R, Nishino T, Nakamae K (1992) Stress transmission in silica particulate epoxy composite by X-ray diffraction. Polymer 33:5167–5172. https://doi.org/https://doi.org/10.1016/0032-3861(92)90796-Y
78. Xu S, Girouard N, Schueneman G et al (2013) Mechanical and thermal properties of waterborne epoxy composites containing cellulose nanocrystals. Polymer 54:6589–6598. https://doi.org/https://doi.org/10.1016/j.polymer.2013.10.011
79. Yang H-S, Kiziltas A, Gardner DJ (2013) Thermal analysis and crystallinity study of cellulose nanofibril-filled polypropylene composites. J Therm Anal Calorim 113:673–682. https://doi.org/10.1007/s10973-012-2770-z

80. Young RJ, Eichhorn SJ (2007) Deformation mechanisms in polymer fibres and nanocomposites. Polymer 48:2–18. https://doi.org/https://doi.org/10.1016/j.polymer.2006.11.016
81. Young RJ, Kinloch IA, Gong L, Novoselov KS (2012) The mechanics of graphene nanocomposites: A review. Compos Sci Technol 72:1459–1476. https://doi.org/https://doi.org/10.1016/j.compscitech.2012.05.005
82. Zhai L, Kim HC, Kim JW et al (2018) Elastic moduli of cellulose nanofibers isolated from various cellulose resources by using aqueous counter collision. Cellulose 25:4261–4268. https://doi.org/10.1007/s10570-018-1836-x

Figures

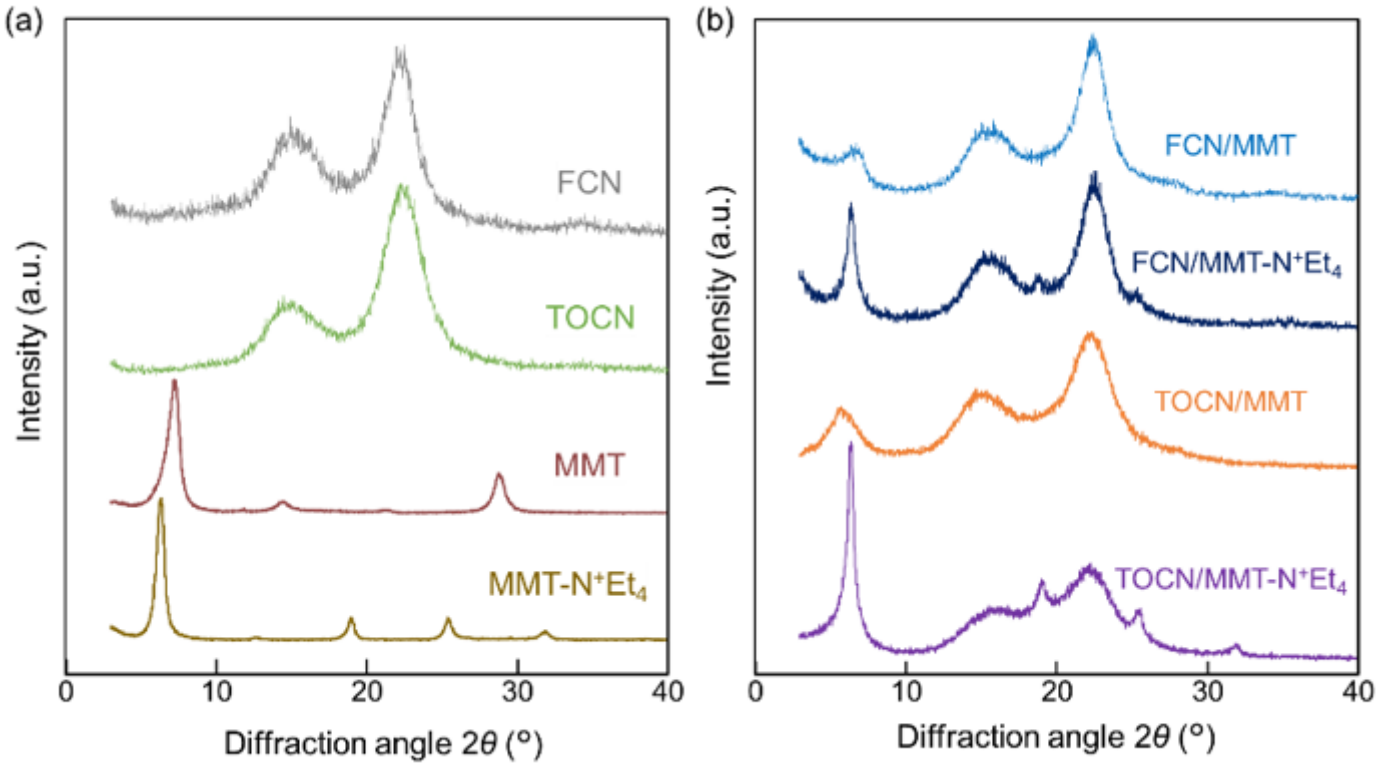

Figure 1

X-ray diffraction profiles of (a) FCN, TOCN, MMT and MMT-NEt4+, and (b) FCN/MMT, FCN/MMT-N+Et4, TOCN/MMT and TOCN/MMT-N+Et4 composites.

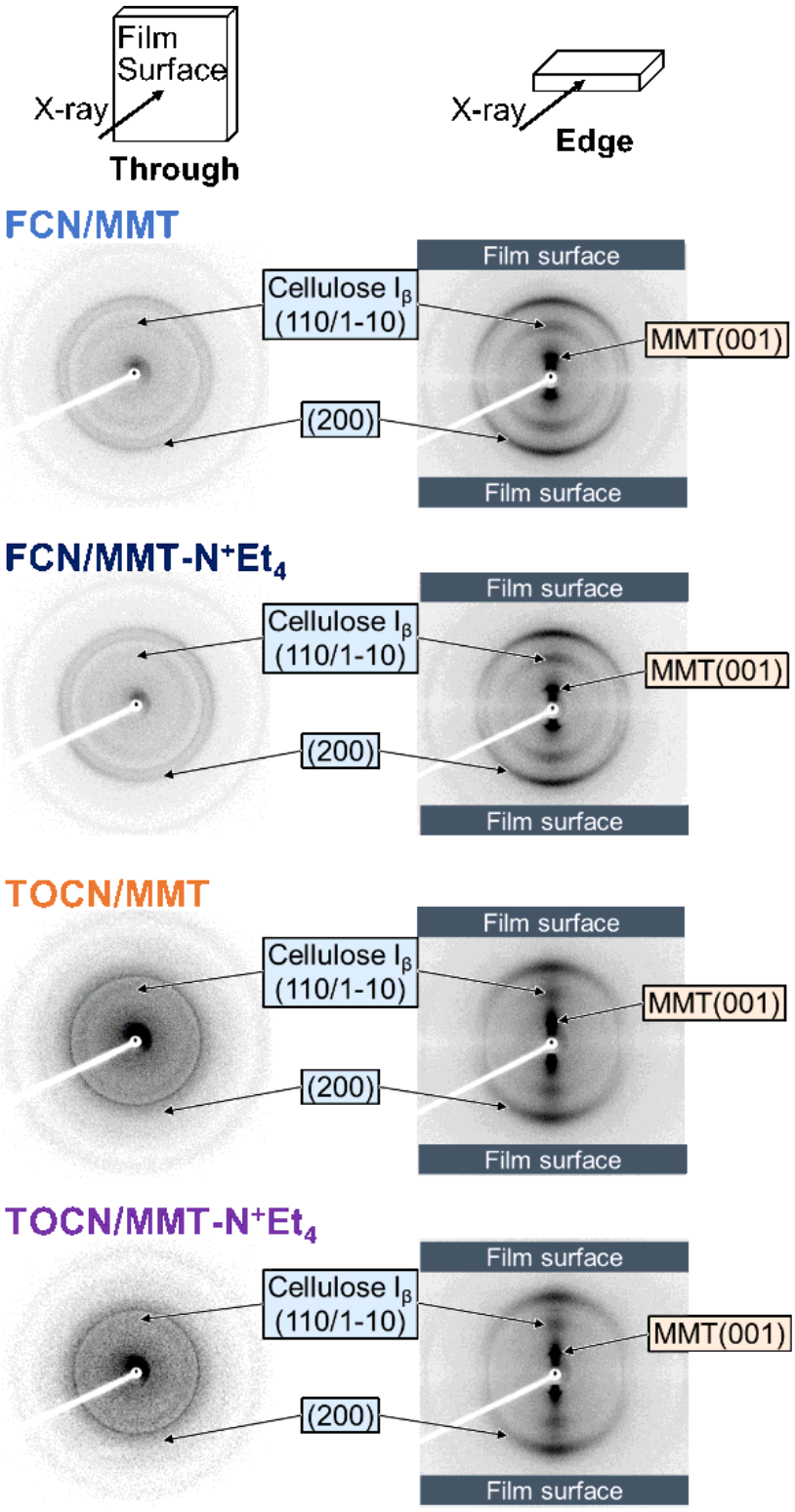

Figure 2

2D X-ray diffraction photographs of FCN/MMT, FCN/MMT-N+Et4, TOCN/MMT and TOCN/MMT-N+Et4 composites.

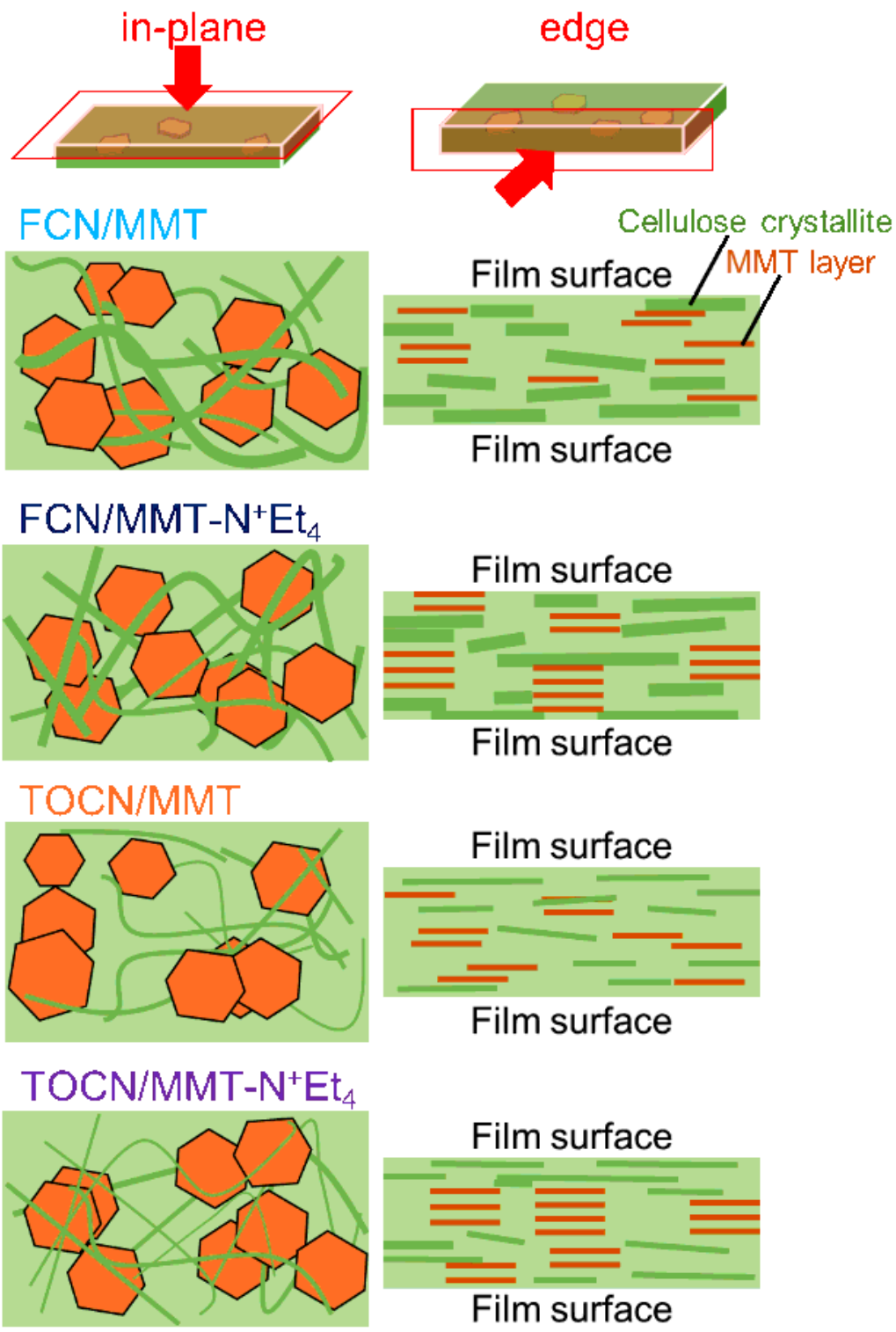

Figure 3

Schematic structure model of CNF matrixes and MMT fillers in the composites.

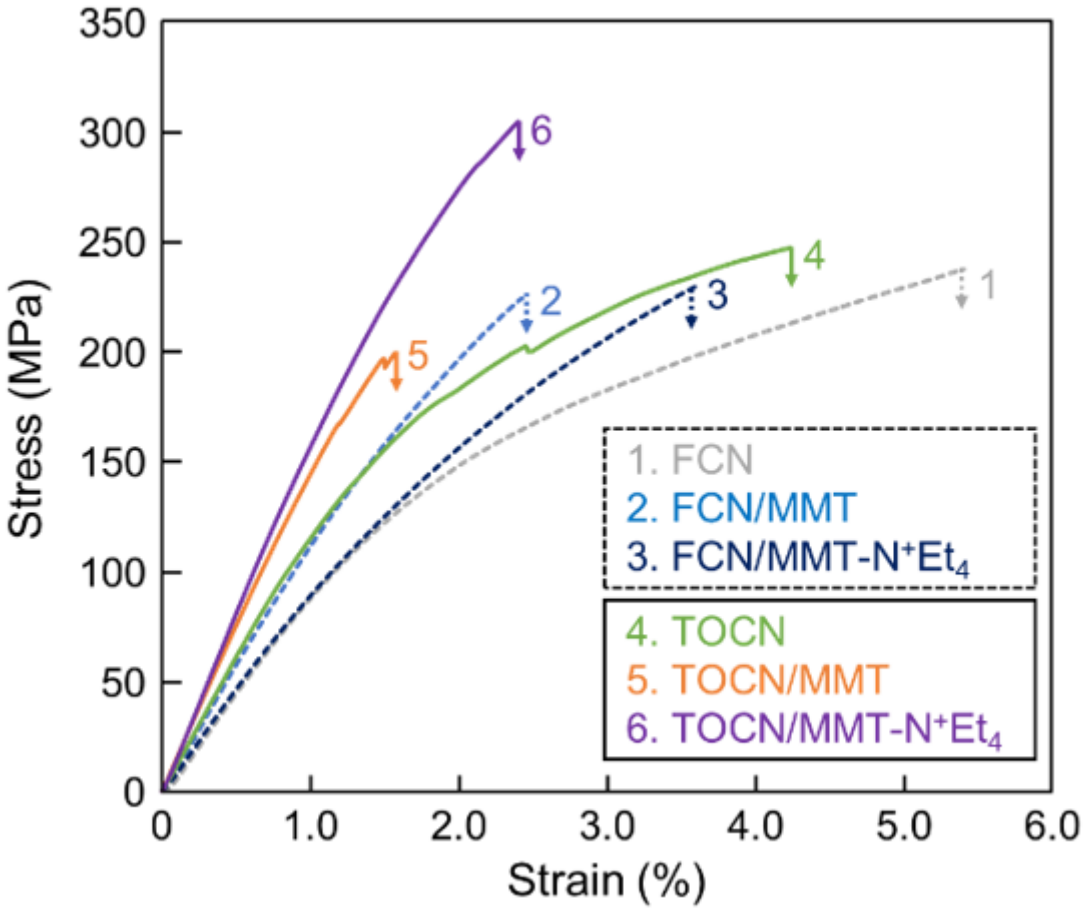

Figure 4

Stress-strain curves of FCN, FCN/MMT, FCN/MMT-N+Et4, TOCN, TOCN/MMT, and TOCN/MMT-N+Et4 films.

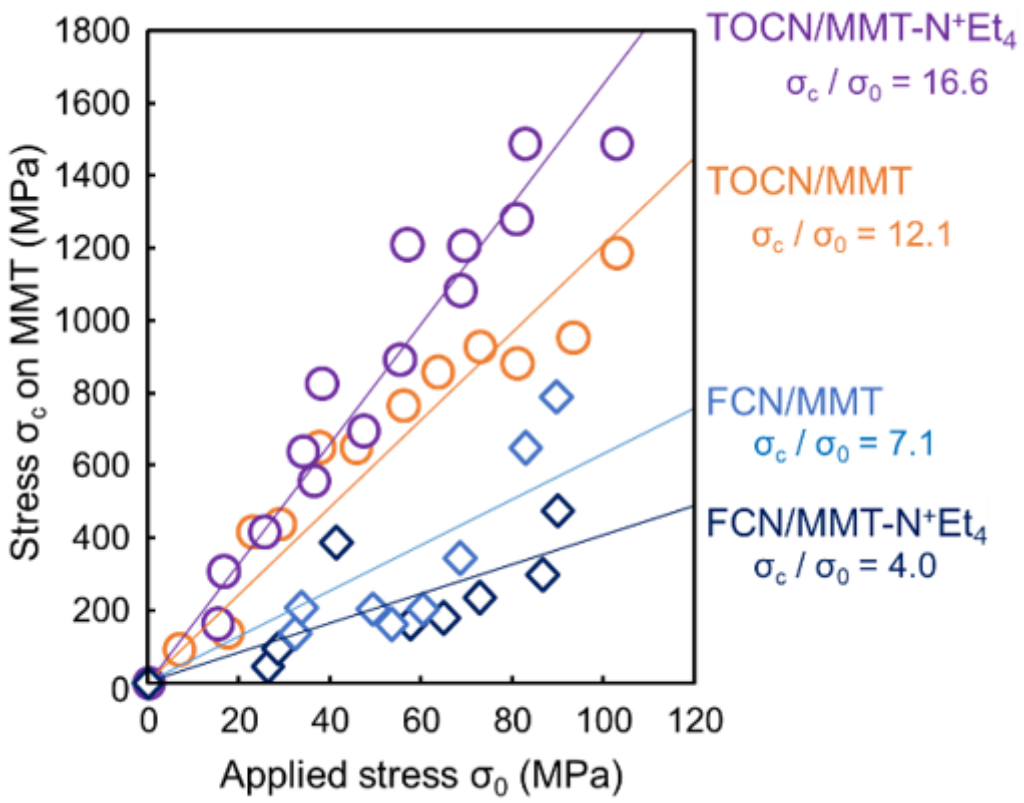

Figure 5

Relationship between the stress σ0 applied to the FCN/MMT, FCN/MMT-N+Et4, TOCN/MMT and TOCN/MMT-N+Et4, and the stress σc on the MMT crystallites, and their stress transfer coefficients σc/σ0.

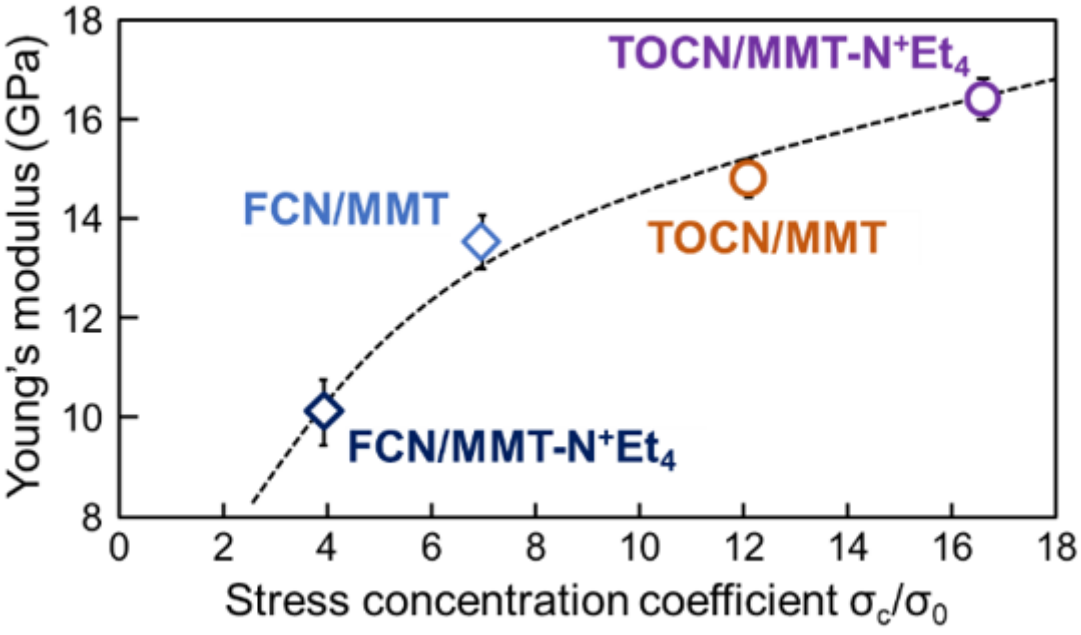

Figure 6

Stress transfer coefficients and Young’s modulus of FCN/MMT, FCN/MMT-N+Et4, TOCN/MMT and TOCN/MMT-N+Et4 composites.

Supplementary Files

This is a list of supplementary files associated with this preprint. Click to download.

- Graphicalabstract.png
- CNFMMTsupporting3.docx